







Communication

Covalently Cross-Linked Nanoparticles Based on Ferulated Arabinoxylans Recovered from a Distiller's Dried Grains Byproduct

Yubia De Anda-Flores ¹, Elizabeth Carvajal-Millan ^{1,*}, Jaime Lizardi-Mendoza ¹, Agustín Rascon-Chu ², Ana Luisa Martínez-López ³, Jorge Marquez-Escalante ¹, Francisco Brown-Bojorquez ⁴ and Judith Tanori-Cordova ⁴

¹ Biopolymers-CTAOA, Research Center for Food and Development (CIAD, A.C.), Carretera Gustavo Enrique Astiazaran Rosas No. 46, Hermosillo 83304, Sonora, Mexico; yubia.deanda@estudiantes.ciad.mx (Y.D.A.-F.); jalim@ciad.mx (J.L.-M.); marquez1jorge@gmail.com (J.M.-E.)

² Biotechnology-CTAOV, Research Center for Food and Development (CIAD, A.C.), Carretera Gustavo Enrique Astiazaran Rosas No. 46, Hermosillo 83304, Sonora, Mexico; arascon@ciad.mx

³ NANO-VAC Research Group, Department of Chemistry and Pharmaceutical Technology, University of Navarra, 31008 Pamplona, Spain; amlopez@unav.es

⁴ Department of Polymers and Materials Research, University of Sonora, Hermosillo 83000, Sonora, Mexico; francisco.brown@unison.mx (F.B.-B.); jtanori@unison.mx (J.T.-C.)

* Correspondence: ecarvajal@ciad.mx; Tel.: +52-662-289-2400

Received: 20 May 2020; Accepted: 11 June 2020; Published: 13 June 2020



Abstract: The purpose of this investigation was to extract ferulated arabinoxylans (AX) from dried distillers' grains with solubles (DDGS) plus to investigate their capability to form covalently cross-linked nanoparticles. AX registered 7.3 µg of ferulic acid/mg polysaccharide and molecular weight and intrinsic viscosity of 661 kDa and 149 mL/g, correspondingly. Fourier transform infrared spectroscopy (FTIR) was used to confirm the identity of this polysaccharide. AX formed laccase induced covalent gels at 1% (*w/v*), which registered an elastic modulus of 224 Pa and a content of FA dimers of 1.5 µg/mg polysaccharide. Scanning electron microscopy pictures of AX gels exhibited a microstructure resembling a rough honeycomb. AX formed covalently cross-linked nanoparticles (NAX) by coaxial electrospray. The average hydrodynamic diameter of NAX determined by dynamic light scattering was 328 nm. NAX presented a spherical and regular shape by transmission electron microscopy analysis. NAX may be an attractive material for pharmaceutical and biomedical applications and an option in sustainable DDGS use.

Keywords: ferulated arabinoxylans; cross-linking; electrospray; nanoparticles; bioethanol industry

1. Introduction

Arabinoxylans (AX) are cell wall polysaccharides present in the outer layer and the endosperm of cereal grains [1]. The AX from grains endosperm are water-extractable (WEAX), while those recovered from pericarp through chemical or enzymatic treatments are water unextractable (WUAX) [2,3]. AX can be retrieved from several maize byproducts such as maize wastewater (nejayote) and distiller's dried grains with solubles (DDGS) [4–6]. DDGS has been considered an attractive source of AX [7–9]. AX polymeric backbone is based on xylose (β -1,4 linkages) and α -L-arabinose substitutions (α -1,3 and/or α -1,2). Arabinose can be esterified with ferulic acid (FA) on O-5 position (Figure 1) [1,7,8]. AX are able to develop covalent gels by FA oxidative coupling by chemical (ferric chloride, ammonium persulfate, among others) or enzymatic (peroxidase, laccase, among others) cross-linkers [9]. The AX

cross-linking structures are dimers of FA (di-FA) (8–5' benzo, 5–5', 8–5', 8–O–4' and 8–8' isomers) and trimer of FA (tri-FA) (4–O–8', 5' 5'' dehydrotriferulic acid).

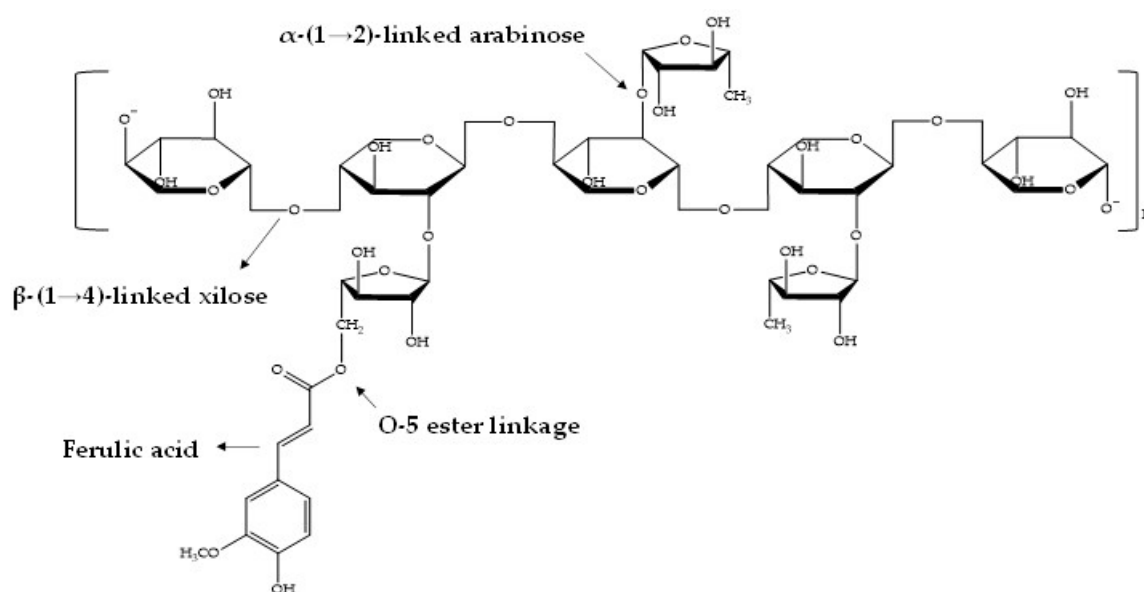


Figure 1. Chemical structure of ferulated arabinoxylan.

Physical interactions among the AX chains can also participate in the cross-linking mechanism defining gel's features [8]. AX gelling capability is related to the polysaccharide structural characteristics, for instance, molecular weight (Mw), arabinose to xylose proportion (A/X) and FA amount [8]. AX have been used to fabricate different cross-linked materials such as hydrogels [8], aerogels [10], films [11], beads [12], microspheres [13]—and more recently, nanoparticles [14]. These diverse AX materials have been used to encapsulate different bioactive molecules and microorganisms for pharmaceutical, biomedical, food technology and postharvest disease applications, among others. Polysaccharide nanoparticles can be fabricated by using different methods such as self-assembly [15], ionic gelation [16], complex coacervation [17], nanoemulsions [18], desolvation [19], spray-drying [20] and electrospraying [21]. The electrospraying technique can atomize a liquid using an electric field. The electric field is capable of overcoming the cohesion force of the dispersions that drip from the needle in a jet form. Then, it was possible to break the surface tension causing the droplets to break up into smaller droplets, which migrate as a function of an electrical potential allowing their recovery as nanoparticles [21–23]. In this regard, the formation of AX covalently cross-linked nanoparticles (NAX) is favored by a high content of FA in the molecule, as reported in a previous study where AX containing 12 $\mu\text{g}/\text{mg}$ polysaccharide allowed the formation of nanoparticles [14]. However, the AX used in that study [14] were extracted from a maize pericarp recovered intact from maize grain (not previously exposed to any other chemical or enzymatic process), which may imply an uncommon and complicated industrial process. As far as we are aware, the formation of NAX using an AX extracted from an abundant and worldwide industrial byproduct such as DDGS has not been described somewhere else. Therefore, the present work targeted to recover AX from DDGS and to investigate their ability to form covalently cross-linked nanoparticles.

2. Materials and Methods

2.1. Materials and Reagents

DDGS (dried distillers' grains with solubles remaining after the starch fraction of maize) was acquired from a feed distributor in Mexico. Laccase (E.C.1.10.3.2) source was *Trametes versicolor*. All chemicals used were obtained from Sigma-Aldrich Co. (St. Louis, MO, USA).

2.2. AX Recovery

AX were obtained by alkaline hydrolysis as reported before [4], with some modifications. Sample (100 g) was added to 500 mL of ethanol under stirring at 100 rpm at 25 °C for 12 h. The solids were filtrated (2.7 µm), collocated in 700 mL of distilled water and heated at 100 °C for 30 min. After that, the solids were filtrated (2.7 µm) and hydrolyzed with 500 mL of 0.5-N NaOH solution at 25 °C for 15 min under shaking (100 rpm) and obscurity. The liquid phase was acidified at pH 4 with 3-N HCl, centrifuged (12,096× g, 20 °C, 15 min). The polysaccharide was recuperated after solvent exchange in ethanol (80% *v/v*), absolute ethanol and acetone. The resulting AX was stored as a powder.

2.3. AX Characterization

2.3.1. FA, di-FA and tri-FA Contents

FA, di-FA and tri-FA contents in AX and cross-linked AX were determined by high performance liquid chromatography as formerly informed [8,24] using an Alltima C18 column (250 × 4.6 mm; Alltech Associates, Inc., Deerfield, IL, USA) and a photodiode array detector Waters 996 (Millipore Co., Milford, MA, USA). Detection was followed by UV absorbance at 320 nm using acetonitrile and sodium acetate buffer (0.05 M at pH 4.0) as gradient elution at 1 mL/min at 35 °C, in linear gradients from 15/85 to 35/65 in 30 min, 35/65 to 60/40 in 0.5 min, 60/40 to 15/85 in 4.5 min and finally maintained at 15/85 for 5 min.

2.3.2. Fourier Transform Infrared Spectroscopy (FTIR)

AX was placed on an ATR module and FTIR spectrum was obtained in absorbance mode (4000–400 cm⁻¹) [25] using a Nicolet iS50 FTIR spectrometer (Nicolet Instrument Corp., Madison, WI, USA).

2.3.3. Macromolecular Characteristics

The AX weight-average molar mass (M_w), intrinsic viscosity ($[\eta]$) and polydispersity index ($I = M_w/M_n$) were determined. A size exclusion chromatography system coupled to a DAWN HELOS-II 8 multi-angle laser light scattering (MALLS), a ViscoStar-II viscometer, and a refractive index (RI) Optilab T-rex detector was used (Wyatt Technology Corp., Santa Barbara, CA, USA). Sample was dispersed (5 mg/mL) in 50-mM NaNO₃/0.02% NaN₃; centrifuged (15,000 rpm, 20 °C, 10 min) and filtered (0.45 µm). The sample was injected (0.7 mL/min) onto an Agilent HPLC System (G1310B Iso-Pump, G1329B autosampler and G1314F variable wavelength detector, Agilent Technologies, Inc., Santa Clara, CA, USA). Shodex OH-pak SBH-Q-804 and 805 (Shodex Showa Denco K.K., Tokyo, Japan) columns were utilized. The software ASTRA 6.1 and a specific refractive index increment (dn/dc) of 0.146 mL/g were used [26].

2.3.4. Gelation

The gelling process of AX dispersion (1% *w/v*) in 0.1 M acetate phosphate buffer (pH 5.5) containing laccase (1.675 nkat/mg polysaccharide) was investigated by using a small deformation oscillatory rheometer (Discovery HR-2; TA Instruments, New Castle, DE, USA) [8]. AX cross-linking was registered at 0.25 Hz and 5% strain for 90 min at 25 °C. Mechanical (0.01–10 Hz) and strain (0.02%–20%) spectra were recorded in the gel formed.

2.3.5. Scanning Electron Microscopy (SEM) Analysis

AX powder coated with gold was analyzed in a microscope JEOL 5410LV (JEOL, Peabody, MA, USA) under a high vacuum, 20 kV accelerating voltage, and using secondary electron detector. To study the external morphology of the AX powder, ImageJ software was used.

2.4. Arabinoxylan Nanoparticles (NAX) Preparation

NAX were obtained by the coaxial electrospray technique (Profector Life Science, Dublin, Ireland) [27], as shown in the experimental diagram (Figure 2). The AX dispersion at 1% (*w/v*) in 0.1-M acetate phosphate buffer at pH 5.5 was used in the internal syringe and the laccase dispersion (1.675 nkat/mg sample) in the outer syringe. The dispersions were injected and flowed through the inner (AX) and external (laccase) capillaries at 1 mL/h using two pumps (WorldPrecision Instruments, AL-1000, Sarasota, FL, USA). The distance from the needle tip to the glass collector was 7 cm. A voltage of 10 kV was used. NAX were recovered in mineral oil at 500 rpm for 24 h at 25 °C. Mature NAX were washed with ultrapure water, vortexed (1 min), then centrifuged (2000× *g*, 10 min, 20 °C).

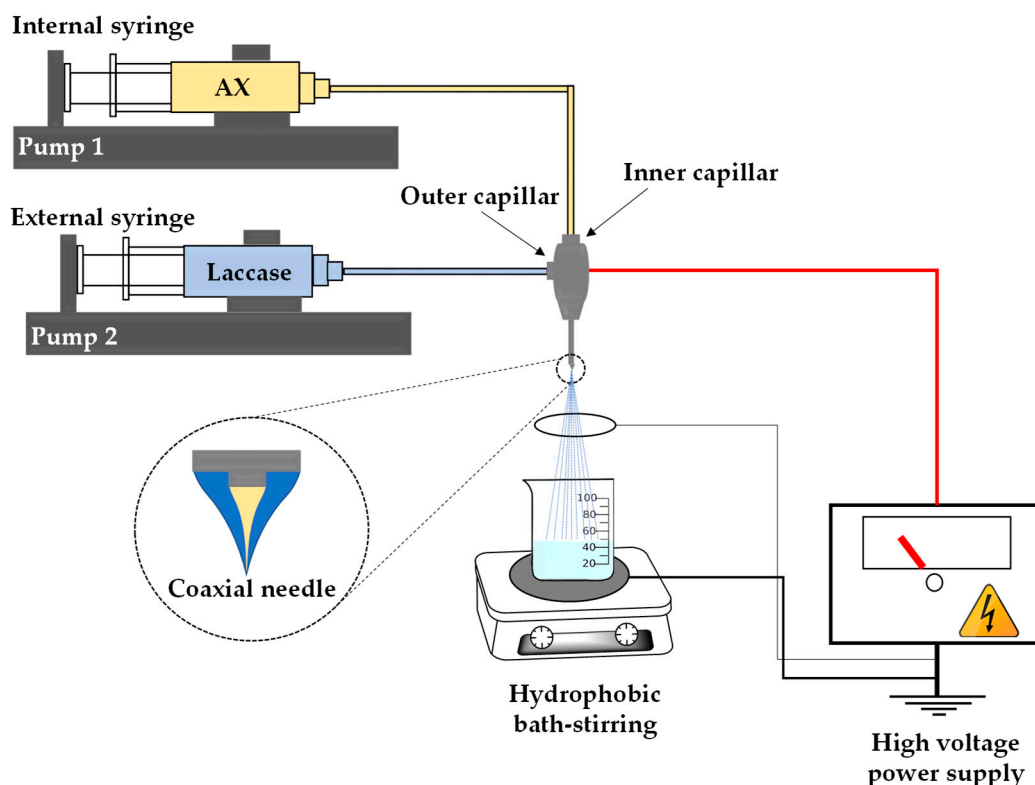


Figure 2. Representation of cross-linked nanoparticles (NAX) fabrication by coaxial electrospray method.

2.5. NAX Characterization

2.5.1. Dynamic Light Scattering (DLS)

NAX size plus size distribution were analyzed by DLS on a Möbiuž (Wyatt Technology Corp., Santa Barbara, CA, USA) at 532 nm and a detection angle of 163.5°. A NAX suspension (0.3 mg/mL) was used, which was filtered through a 1.4- μm membrane before measurement. Subsequently, the sample was loaded into disposable polystyrene cells for DLS. The software DYNAMICS 7.3.1.15 was used (Wyatt Technology Corp., Santa Barbara, CA, USA).

2.5.2. Transmission Electron Microscopy (TEM) Analysis

The morphology and size of NAX was investigated using a transmission electron microscope at 200 kV (JEM 2010F, JEOL, Ltd., Tokyo, Japan). Exactly 9 μL of NAX resuspended on ultrapure water was deposited on a TEM grid (carbon-coated copper) and let to dry. Phosphotungstic acid was used to perform the negative staining of the sample. The final sample was placed and dried on a vacuum system before observation [28].

2.6. Statistical Analysis

The analysis was achieved in triplicates, and the results were informed as mean and standard deviation.

3. Results and Discussion

3.1. AX Recovery

The yield of AX removed after 15 min of alkaline hydrolysis was $1.6 \pm 0.1\%$ (w AX/w DDGS, dry weight), which is lower than those reported in previous investigations by using 60 min (4.7% w AX/w DDGS) and 30 min (2.5% w AX/w DDGS) of DDGS alkaline hydrolysis [25,29]. In several studies, it has been found that a short time of alkali extraction decreases AX yield from cereal sources [1,4]. It is essential to mention that some AX sources, such as wheat flour, present lower yield value (0.5% w AX/w wheat flour), and the extraction process is more expensive because the use of enzymes is required [9]. In the present study, the extraction of AX from DDGS did not involve enzymes, and the polysaccharide is recovered from an industrial byproduct.

3.2. AX Characterization

3.2.1. Phenolic Acids

The AX recovered in the present research registered an FA content of $7.30 \pm 0.20 \mu\text{g FA/mg polysaccharide}$, which was higher than the value found in AX extracted with alkaline hydrolysis of 60 min ($3.30 \pm 0.46 \mu\text{g FA/mg polysaccharide}$) [25], but similar to AX with 30 min of alkali extraction ($7.50 \pm 0.60 \mu\text{g FA/mg polysaccharide}$) [29]. Alkali treatments cleave the bonds that link hemicellulose, cellulose and lignin in the cereals cell walls, allowing AX extraction [30]. However, FA, di-FA, and tri-FA ester-linked to AX can also be partially removed during alkaline treatment, as ester bonds are highly labile in alkali (saponification) [31]. It has been reported that long periods of alkaline treatment during AX extraction reduce the polysaccharide molecular weight and FA content [4,8]. In previous studies [25,29], the Mw of AX recovered from DDGS by alkaline treatment was lower (200 and 270 kDa) than the value registered in the present study (661 kDa; Table 1). This difference can be attributed to the more extended time of alkali exposure used by those authors (30 and 60 min, respectively), concerning the 15 min used in the present study. The chemical treatment used in the current investigation did not result in a considerable reduction in AX Mw, probably due to the complexity of maize cell walls present in DDGS. The use of harsher alkali treatment would be helpful for substantial enhancement in glycosidic bonds hydrolysis.

In another research [9], wheat AX registered similar FA contents after 10 ($1.96 \pm 0.10 \mu\text{g/mg polysaccharide}$) and 20 min ($1.83 \pm 0.16 \mu\text{g/mg polysaccharide}$) of exposure at 1% (*w/v*) lime at 20 °C, registering. In addition, a decrease in the polysaccharide intrinsic viscosity ($[\eta]$) value from 6.42 ± 0.16 to $5.75 \pm 0.81 \text{ dL/g}$. Similarly, the alkaline hydrolysis conditions used in the present investigation allowed using DDGS to recover AX presenting a FA content close to that registered in the literature by applying 30 min of chemical treatment, but, besides, permitted to conserve a higher Mw in the polysaccharide.

AX extracted in this study contained dimers and trimers of FA (Table 1). These structures have been associated with the occurrence of moderately cross-linked polysaccharide chains [4,32,33]. The 5–5', 8–5' and 8–O–4' di-FA isomers represented 47%, 43% and 10% of the entire di-FA, respectively. A characteristic HPLC chromatogram for phenolic acids in AX is presented in Figure 3. The prevalence of 5–5' di-FA in maize AX was reported in several studies [4,29,34]. The di-FA content found in the current research was minor than those described in AX extracted from DDGS with 30 and 60 min of alkaline treatment (0.30–0.56 $\mu\text{g/mg AX}$), but the proportions of 5–5', 8–5' and 8–O–4' di-FA isomers were similar [4,25,29,32]. It has been reported that maize AX present decoration with ferulated (FA, di-FA) oligosaccharidic side-chains [35]. It is possible that the short time of alkaline treatment used in the current study favored the removal of these ferulated AX side-chains resulting in a loss of FA

and di-FA content and a high molecular weight polysaccharide. The A/X value (1.2) found in this work was close to that reported in other studies using the same AX source ($A/X = 1.1$) and indicated a highly branched structure [29]. Other authors have reported A/X values for maize bran ranging from 0.72 to 0.85, corresponding to a moderately branched structure [4,36]. Polydispersity index (I) value registered for AX was in the range informed in the literature for further AX from DDGS [37].

Table 1. Macromolecular characteristics of AX extracted from distillers' grains with solubles (DDGS).

Component	Value
FA ($\mu\text{g}/\text{mg}$ AX) ¹	7.30 ± 0.20
Total, di-FA ($\mu\text{g}/\text{mg}$ AX) ¹	0.212 ± 0.009
5,5'	0.100 ± 0.005
8-5'	0.090 ± 0.002
8-O-4'	0.021 ± 0.006
tri-FA ($\mu\text{g}/\text{mg}$ AX)	traces
A/X ratio ¹	1.2
Molecular weight (Mw) kDa ²	661
Polydispersity index $I = (Mw/Mn)$ ²	2.4
Intrinsic viscosity $[\eta]$ (mL/g) ²	149

¹ mean value of triplicate determinations \pm standard deviation. ² Absolute values.

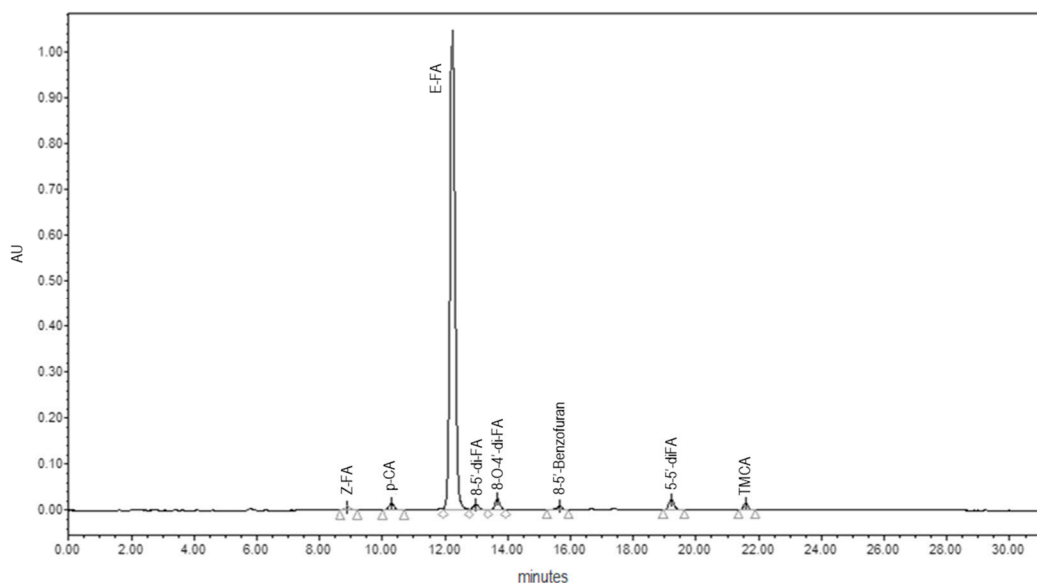


Figure 3. HPLC chromatogram of phenolic acids for ferulated arabinoxylans (AX) sample.

3.2.2. FTIR Spectroscopy

The FTIR spectrum of AX powder extracted in this present work (Figure 4) presented a pattern comparable to that previously described for other cereal AX [11,34,38–41]. The absorption bands at $1200\text{--}800\text{ cm}^{-1}$ represent the specific region for polysaccharides [38,39]. A central band is observed at 1035 cm^{-1} , which is related to the C–OH link and a small shoulder at 897 cm^{-1} can be linked to the C–O–C antisymmetric stretch of the β (1→4) glycosidic bond [34,39]. Bands at 1640 and 1533 cm^{-1} are linked to amide I and amide II, correspondingly, indicating the presence of protein [29,40]. The signals at 3292 and 2935 cm^{-1} correspond to the stretching of the OH and CH_2 groups, respectively [11,41].

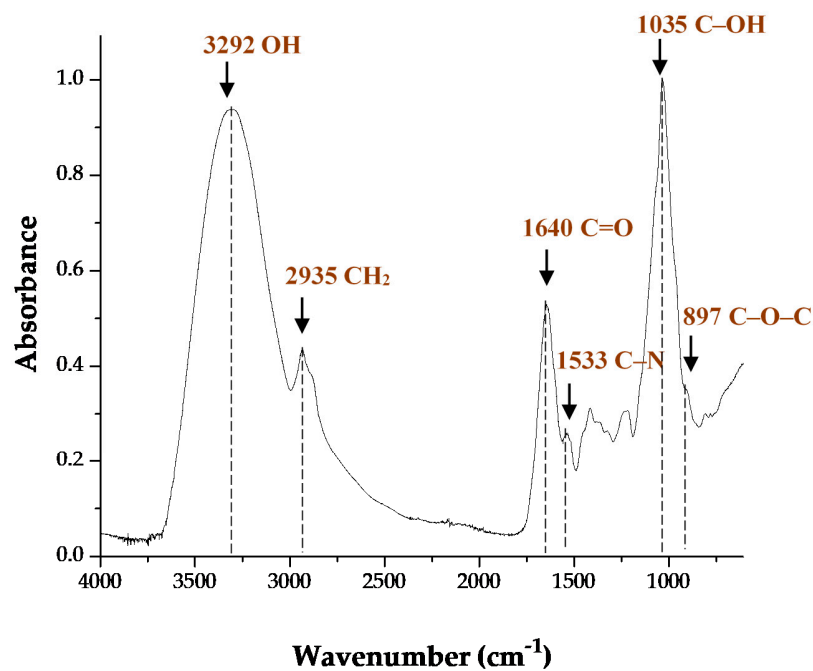


Figure 4. FTIR spectrum of AX from distillers' grains with solubles (DDGS).

3.2.3. Microstructure of AX powder

SEM analysis revealed the morphology of AX powder (Figure 5). The sample presented aggregated particles with irregular shapes and rough surfaces. The size of particles found was heterogeneous and around 30–170 μm of length. These morphologic characteristics can be attributed to the type of drying in which the sample was exposed, as that previously reported for maize bran AX [42].

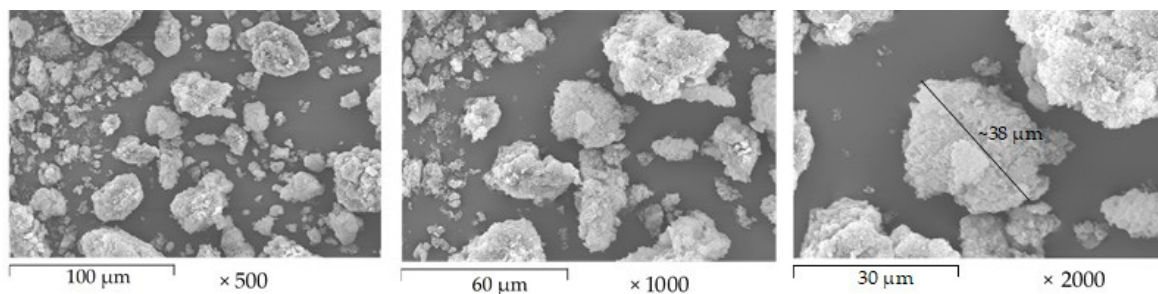


Figure 5. SEM micrographs of AX powder extracted from DDGS. Images at 500, 1000 and 2000 \times magnification.

3.2.4. Gelling of AX

Figure 6a displays the gel formation with elastic (G') modulus increase followed by a flat section and G' higher than viscous modulus (G''). The crossover between the G' and G'' values was at 3 min. The development of an elastic polymeric network could be followed by a decrease in $\tan \delta$ (G''/G') during laccase exposure. In the cured gel (90 min), G' presented a value of 224 Pa. In a previous study [29], a G' value of 767 Pa was reported for 2% (w/v) gels based on AX (7.5 μg FA/mg polysaccharide and 200 kDa) extracted from DDGS. In the present study, it was possible to form gels at 1% (w/v) using AX with similar content of FA, but higher Mw (661 kDa) about the previous report [29]. It has been reported that a high Mw in AX allows forming stronger gels. The higher arabinose to xylose proportion and the content of FA registered in the AX extracted from DDGS in the present research favored the formation of covalent cross-links [8,42].

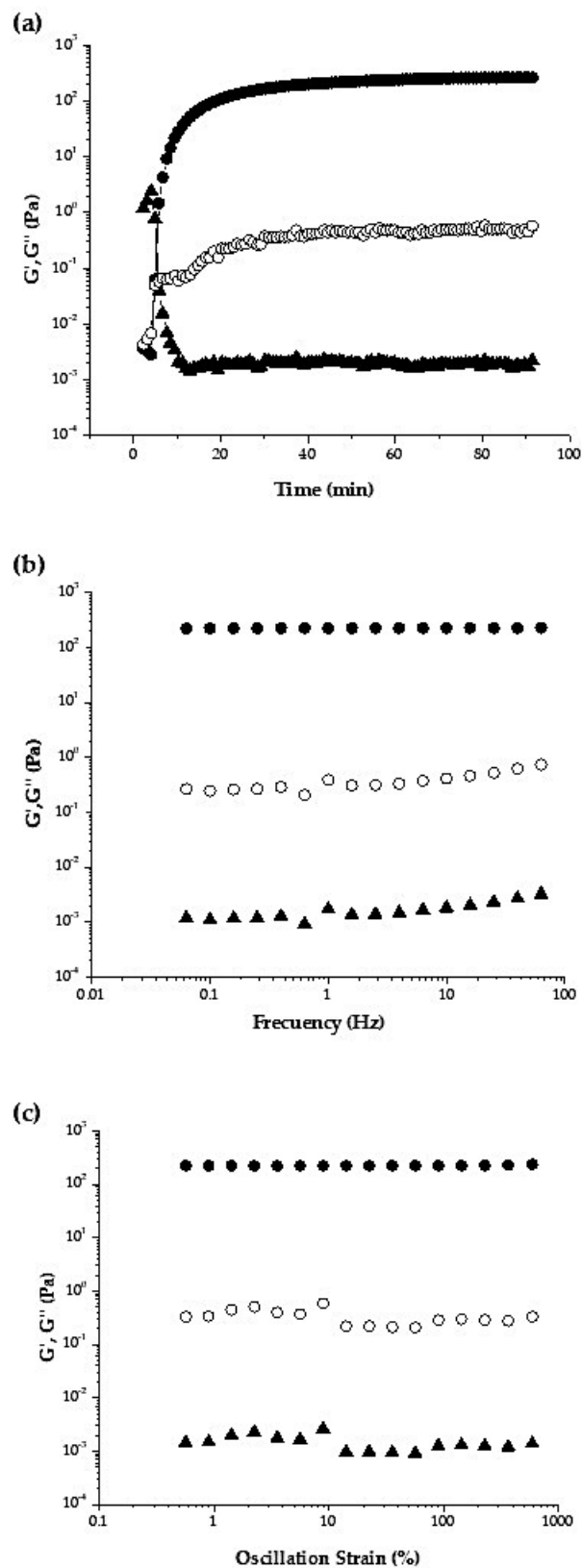


Figure 6. (a) Gelation of 1% (*w/v*) dispersion of AX extracted from DDGS during laccase exposure at 0.25 Hz and 5% strain; (b) mechanical spectrum of 1% (*w/v*) cured AX gels, measurements at 5% strain; (c) Strain sweep of 1% (*w/v*) cured AX gels, measurements at 0.25 Hz. All tests performed at 25 °C. G' (●), G'' (○), $\tan \delta$ (▲).

The gel formed presented a total di-FA of 1.5 $\mu\text{g}/\text{mg}$ AX. The di-FA isomeric forms existing in AX before gelation were 5-5', 8-5' and 8-O-4' at 47, 43 and 10%, respectively. After AX gelation, the 5-5' and 8-O-4' di-FA contents decreased down to 11 and 15%, respectively, while the 8-5' structure increased up to 74%. The prevalence of 8-5' di-FA isomer in AX gels has been observed in AX from different cereals sources [25]. The decrease in 5-5' di-FA content once AX gelled may promote the inter-polysaccharide chain cross-linking as it has been previously reported that 5,5' di-FA may favor the intra-polysaccharide chain bonds [43]. This result suggests that the AX gel formed developed an interconnected polymeric network structure.

Laccase induced AX gel mechanical spectrum is displayed in Figure 6b. The G' values were linear and independent over the entire frequency range and prevailed over G'' during the test, confirming a typical solid-like behavior. Figure 6c shows the strain spectrum of AX gels, with elastic behavior dominating over the viscous one ($G' > G''$) and $\tan \delta$ (G''/G') values below 1, indicating a gel-like consistency in the strain range investigated. Both frequency and strain spectra are similar to the results reported in previous studies [25,32,44,45]. These data confirm that below the rheological conditions used in the present study, AX gel is stable, the structure is not easily disturbed.

3.3. AX Nanoparticles (NAX) Preparation and Characterization

The coaxial electrospray allowed the formation of NAX, which was collected in a hydrophobic bed of mineral oil to permit their maturation and avoid coalescence. Afterward, NAX were in constant stirring for 24 h until their subsequent recovery. The AX dispersion at 1% (w/v) facilitated the formation of small drops in comparison with previous electrosprayed AX microspheres and beads formed at higher AX concentrations ranging from 2% to 8% (w/v) [46].

3.3.1. Size Distribution of NAX

The size, distribution and polydispersity index (PDI) of the NAX obtained through coaxial electrospray under the conditions used were determined by DLS. Figure 7 shows the NAX size distribution as a function of the relative amount of light emitted by each population (% Intensity) in an aqueous medium. According to the DLS measurements, the average hydrodynamic diameter and the PDI of NAX were 328 ± 25 nm and 0.2, respectively.

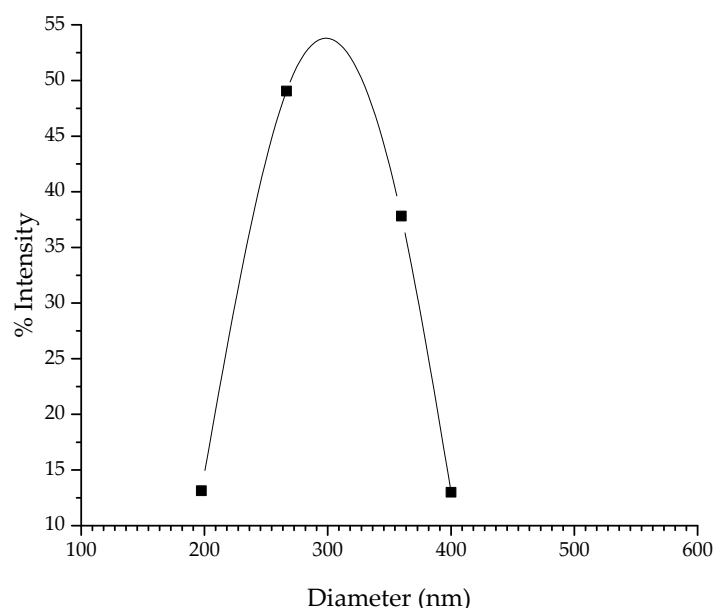


Figure 7. Size distribution of NAX as a function of the relative amount of light emitted by each population (% Intensity).

In a previous study [14], nanoparticles formed using maize pericarp AX presented a diameter of 193 ± 7 nm and a PDI of 0.1, which may be associated with the higher amount of FA ($12 \mu\text{g}/\text{mg}$ AX) and polysaccharide concentration employed (2% *w/v*) respect to present study ($7.3 \mu\text{g}/\text{mg}$ AX and 1% *w/v*, respectively). The formation of smaller droplets by using coaxial electrospray in combination with a rapid laccase induced gelation of AX from DDGS allowed the formation of gelled nanoparticles. The cross-linking agent placed in the external syringe of the coaxial electrospray system permitted to start the AX gelation from the outer part of the material towards the center, generating a protective layer [27,44]. Coaxial electrospray system helped to reduce the aggregation of the AX gelled drops letting the generation of particles in the nanometric scale [46].

3.3.2. Morphology of NAX

The morphologic characterization of NAX was performed by TEM using negative 1% (*w/v*) phosphotungstic acid staining. The generation of a negative contrast allows observing NAX as light objects in a dark environment. NAX presented a spherical shape, as shown in the TEM image (Figure 8). Size measurements of individual particles were in the range of 67–335. The size of some NAX estimated from TEM was smaller than that registered by DLS because the latter technique calculates the hydrodynamic diameter of the particles in the hydrated state. While that, TEM is performed in dry particles, and consequently, the loss of water reduces their size. The dimensions of the NAX formed are similar to those reported for particles based on other polysaccharides [18,47–51].

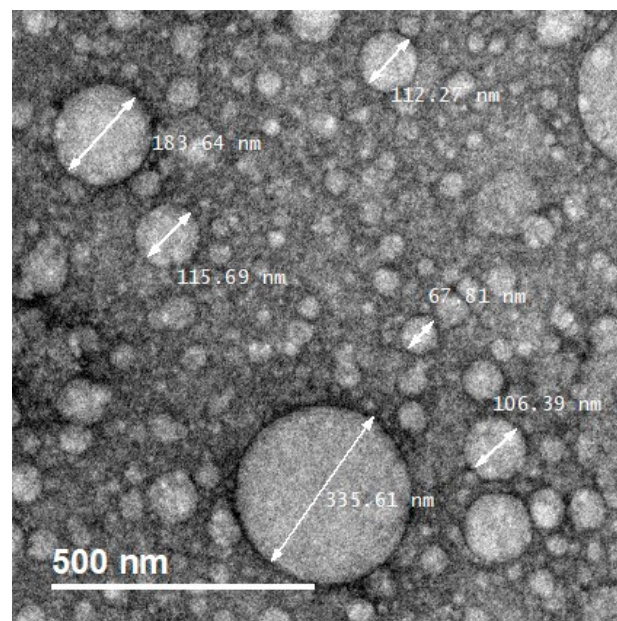


Figure 8. TEM micrographs of NAX based on AX from DDGS.

The results obtained in this study show that AX extracted from DDGS allow the formation of NAX by coaxial electrospray. In addition, the high FA content in the AX used allowed rapid gelation of the droplets, maintaining essential characteristics of the gelled particles, such as a low degree of aggregation, spherical shape and sizes on the nanometric scale.

In general, it is considered that polysaccharide nanoparticles offer advantages such as biocompatibility and biodegradability. In this regard, the development of polysaccharide nanoparticles has been of interest because these materials can be used to encapsulate and deliver molecules to target sites decreasing side effects [50]. Therefore, in the present investigation, the formation of NAX by using an AX recovered from an industrial byproduct such as DDGS represents an excellent opportunity for upcycling bioethanol waste and produce a nanomaterial with potential high-value applications in pharmaceutical and biomedical areas.

4. Conclusions

AX extracted from DDGS can be used to form covalently cross-linked nanoparticles by the coaxial electrospray method. The nanoparticles of AX produced by this method present a spherical form with an average hydrodynamic diameter and a polydispersity index of 328 nm and 0.2, respectively. These morphologic characteristics in nanoparticles based on AX from DDGS could offer advantages over other AX-based materials intended for drug delivery systems. For example, cell internalization when required and feasibility of variable routes of administration, among others. Therefore, the formation of NAX using AX from DDGS could reflect both long term bioethanol waste disposal and production of attractive improved nanomaterial fabrication with potential pharmaceutical and biomedical applications such as colon targeted drug delivery.

Author Contributions: This publication is part of Y.D.A.-F. Ph.D. thesis, which is supervised by E.C.-M.; Y.D.A.-F. and E.C.-M. designed and performed the experiments; A.R.-C., J.L.-M., J.T.-C. and A.L.M.-L. are Ph.D. thesis committee of Y.D.A.-F. and assisted in the research providing supervision, software, reagents, materials and laboratory equipment. F.B.-B. performed scanning electron microscopy and J.M.-E. contributed to the methodology and software analysis. All authors have read and agreed on this manuscript.

Funding: This research was funded by 'Fund to support research on the Sonora-Arizona region 2019' Grant Number 20614.

Acknowledgments: The authors are pleased to acknowledge Alma C. Campa and Karla G. Martinez for technical support in Biopolymers laboratory; to J. Alfonso Sánchez Villegas for technical assistance in the electrospray system and to Eduardo A. Larios for transmission electron microscopy analysis. The TEM experiments were performed at the TEM Laboratory of the University of Sonora.

Conflicts of Interest: The authors declare no conflicts of interest.

References

1. Zhang, Z.; Smith, C.; Li, W. Extraction and modification technology of arabinoxylans from cereal by-products: A critical review. *Food Res. Int.* **2014**, *65*, 423–436. [[CrossRef](#)]
2. Saulnier, L.; Guillon, F.; Sado, P.-E.; Chateigner-Boutin, A.-L.; Rouau, X. Plant Cell Wall Polysaccharides in Storage Organs: Xylans (Food Applications). In *Reference Module in Chemistry, Molecular Sciences and Chemical Engineering*; Elsevier: Amsterdam, The Netherlands, 2013.
3. Kiszonas, A.; Fuerst, E.P.; Morris, C.F. Wheat Arabinoxylan Structure Provides Insight into Function. *Cereal Chem. J.* **2013**, *90*, 387–395. [[CrossRef](#)]
4. Carvajal-Millan, E.; Rascón-Chu, A.; Marquez-Escalante, J.; Micard, V.; De León, N.P.; Gardea, A. Maize bran gum: Extraction, characterization and functional properties. *Carbohydr. Polym.* **2007**, *69*, 280–285. [[CrossRef](#)]
5. Chatzifragkou, A.; Charalampopoulos, D. Distiller's dried grains with solubles (DDGS) and intermediate products as starting materials in biorefinery strategies. In *Sustainable Recovery and Reutilization of Cereal Processing By-Products*; Elsevier: Amsterdam, The Netherlands, 2018; pp. 63–86.
6. Rodríguez, V.; Revilla, P.; Ordás, B. New Perspectives in Maize Breeding. In *Maize Cultivation, Uses and Health Benefits*; Jimenez-lopez, J.C., Ed.; Nova Science Publishers, Inc.: Hauppauge, NY, USA, 2012; pp. 27–48.
7. Reis, S.F.; Coelho, E.; Coimbra, M.A.; Abu-Ghannam, N. Influence of grain particle sizes on the structure of arabinoxylans from brewer's spent grain. *Carbohydr. Polym.* **2015**, *130*, 222–226. [[CrossRef](#)] [[PubMed](#)]
8. Carvajal-Millan, E.; Landillon, V.; Morel, M.-H.; Rouau, X.; Doublier, J.-L.; Micard, V. Arabinoxylan Gels: Impact of the Feruloylation Degree on Their Structure and Properties. *Biomacromolecules* **2005**, *6*, 309–317. [[CrossRef](#)] [[PubMed](#)]
9. Figueroa-Espinoza, M.C.; Rouau, X. Oxidative Cross-Linking of Pentosans by a Fungal Laccase and Horseradish Peroxidase: Mechanism of Linkage Between Feruloylated Arabinoxylans. *Cereal Chem. J.* **1998**, *75*, 259–265. [[CrossRef](#)]
10. Marquez-Escalante, J.; Carvajal-Millan, E.; Miki-Yoshida, M.; Álvarez-Contreras, L.; Toledo-Guillén, A.R.; Lizardi-Mendoza, J.; Rascón-Chu, A. Water Extractable Arabinoxylan Aerogels Prepared by Supercritical CO₂ Drying. *Molecules* **2013**, *18*, 5531–5542. [[CrossRef](#)]

11. González, R.; Calderón-Santoyo, M.; Carvajal-Millan, E.; Ascencio, F.; Ragazzo-Sánchez, J.A.; Brown, F.; Rascón-Chu, A. Covalently Cross-Linked Arabinoxylans Films for *Debaryomyces hansenii* Entrapment. *Molecules* **2015**, *20*, 11373–11386. [[CrossRef](#)]
12. Paz-Samaniego, R.; Rascón-Chu, A.; Brown, F.; Carvajal-Millan, E.; Pedroza-Montero, M.R.; Silva-Campa, E.; Sotelo-Cruz, N.; López-Franco, Y.; Lizardi-Mendoza, J. Electrospray-assisted fabrication of core-shell arabinoxylan gel particles for insulin and probiotics entrapment. *J. Appl. Polym. Sci.* **2018**, *135*, 46411. [[CrossRef](#)]
13. Martínez-López, A.L.; Carvajal-Millan, E.; Miki-Yoshida, M.; Álvarez-Contreras, L.; Rascón-Chu, A.; Lizardi-Mendoza, J.; López-Franco, Y. Arabinoxylan Microspheres: Structural and Textural Characteristics. *Molecules* **2013**, *18*, 4640–4650. [[CrossRef](#)]
14. Carvajal-Millan, E.; Rascon-Chu, A.; Morales-Burgos, A.M.; Campa-Mada, A.C.; Martinez-Robison, K.G.; Marquez-Escalante J, T.-G.A.R. Method for the Obtaining Functionalized Arabinoxylans to Form Gelled Nanoparticles Covalent and to Enhance Beneficial Health Effects. Patent Application No. MX/a/2018/007070, 7 June 2018.
15. Sonaje, K.; Lin, Y.-H.; Juang, J.-H.; Wey, S.-P.; Chen, C.-T.; Sung, H.-W. In vivo evaluation of safety and efficacy of self-assembled nanoparticles for oral insulin delivery. *Biomaterials* **2009**, *30*, 2329–2339. [[CrossRef](#)] [[PubMed](#)]
16. Fan, W.; Yan, W.; Xu, Z.; Ni, H. Formation mechanism of monodisperse, low molecular weight chitosan nanoparticles by ionic gelation technique. *Colloids Surf. B Biointerfaces* **2012**, *90*, 21–27. [[CrossRef](#)] [[PubMed](#)]
17. Bajpai, S.; Tankhiwale, R. Investigation of dynamic release of vitamin B2 from calcium alginate/chitosan multilayered beads: Part II. *React. Funct. Polym.* **2006**, *66*, 1565–1574. [[CrossRef](#)]
18. Seidi, F.; Jenjob, R.; Phakkeeree, T.; Crespy, D. Saccharides, oligosaccharides, and polysaccharides nanoparticles for biomedical applications. *J. Control. Release* **2018**, *284*, 188–212. [[CrossRef](#)] [[PubMed](#)]
19. Rao, K.K.; Reddy, P.R.; Lee, Y.-I.; Kim, C. Synthesis and characterization of chitosan–PEG–Ag nanocomposites for antimicrobial application. *Carbohydr. Polym.* **2012**, *87*, 920–925. [[CrossRef](#)]
20. Yang, J.; Han, S.; Zheng, H.; Dong, H.; Liu, J. Preparation and application of micro/nanoparticles based on natural polysaccharides. *Carbohydr. Polym.* **2015**, *123*, 53–66. [[CrossRef](#)]
21. Tapia-Hernández, J.A.; Torres-Chávez, P.I.; Ramírez-Wong, B.; Rascón-Chu, A.; Plascencia-Jatomea, M.; Barreras-Urbina, C.G.; Rangel-Vázquez, N.A.; Rodríguez-Félix, F. Micro- and Nanoparticles by Electrospray: Advances and Applications in Foods. *J. Agric. Food Chem.* **2015**, *63*, 4699–4707. [[CrossRef](#)] [[PubMed](#)]
22. Jaworek, A.; Sobczyk, A.T.; Krupa, A. Electrospray application to powder production and surface coating. *J. Aerosol Sci.* **2018**, *125*, 57–92. [[CrossRef](#)]
23. Lenggoro, W.; Xia, B.; Okuyama, K.; De La Mora, J.F. Sizing of Colloidal Nanoparticles by Electrospray and Differential Mobility Analyzer Methods. *Langmuir* **2002**, *18*, 4584–4591. [[CrossRef](#)]
24. Vansteenkiste, E.; Babot, C.; Rouau, X.; Micard, V. Oxidative gelation of feruloylated arabinoxylan as affected by protein. Influence on protein enzymatic hydrolysis. *Food Hydrocoll.* **2004**, *18*, 557–564. [[CrossRef](#)]
25. Marquez-Escalante, J.; Carvajal-Millan, E. Feruloylated Arabinoxylans from Maize Distiller’s Dried Grains with Solubles: Effect of Feruloyl Esterase on their Macromolecular Characteristics, Gelling, and Antioxidant Properties. *Sustainability* **2019**, *11*, 6449. [[CrossRef](#)]
26. Dervilly-Pinel, G.; Thibault, J.-F.; Saulnier, L. Experimental evidence for a semi-flexible conformation for arabinoxylans. *Carbohydr. Res.* **2001**, *330*, 365–372. [[CrossRef](#)]
27. Rascón-Chu, A.; Baca, J.A.D.; Carvajal-Millan, E.; Pérez, E.; Hotchkiss, A.; González-Ríos, H.; Balandrán-Quintana, R.R.; Campa-Mada, A.C. Electrosprayed Core-Shell Composite Microbeads Based on Pectin-Arabinosylans for Insulin Carrying: Aggregation and Size Dispersion Control. *Polymers* **2018**, *10*, 108. [[CrossRef](#)] [[PubMed](#)]
28. Rochín-Wong, S.; Rosas-Durazo, A.; Zavala-Rivera, P.; Maldonado, A.; Mertinez-Barbosa, M.E.; Vélaz, I.; Córdova, J.T. Drug Release Properties of Diflunisal from Layer-By-Layer Self-Assembled κ -Carrageenan/Chitosan Nanocapsules: Effect of Deposited Layers. *Polymers* **2018**, *10*, 760. [[CrossRef](#)]

29. Mendez-Encinas, M.A.; Carvajal-Millan, E.; Yadav, M.P.; López-Franco, Y.; Rascón-Chu, A.; Lizardi-Mendoza, J.; Brown, F.; Silva-Campa, E.; Pedroza-Montero, M.R. Partial removal of protein associated with arabinoxylans: Impact on the viscoelasticity, crosslinking content, and microstructure of the gels formed. *J. Appl. Polym. Sci.* **2018**, *136*, 136. [[CrossRef](#)]
30. Carvajal-Millan, E.; Guigliarelli, B.; Belle, V.; Rouau, X.; Micard, V. Storage stability of laccase induced arabinoxylan gels. *Carbohydr. Polym.* **2005**, *59*, 181–188. [[CrossRef](#)]
31. Izydorczyk, M.S.; Biliaderis, C.G. Cereal arabinoxylans: Advances in structure and physicochemical properties. *Carbohydr. Polym.* **1995**, *28*, 33–48. [[CrossRef](#)]
32. Kale, M.S.; Hamaker, B.R.; Campanella, O. Alkaline extraction conditions determine gelling properties of corn bran arabinoxylans. *Food Hydrocoll.* **2013**, *31*, 121–126. [[CrossRef](#)]
33. Bunzel, M.; Ralph, J.; Marita, J.M.; Hatfield, R.D.; Steinhart, H. Diferulates as structural components in soluble and insoluble cereal dietary fibre. *J. Sci. Food Agric.* **2001**, *81*, 653–660. [[CrossRef](#)]
34. Morales-Ortega, A.; Carvajal-Millan, E.; López-Franco, Y.; Rascón-Chu, A.; Lizardi-Mendoza, J.; Torres-Chávez, P.; Campa-Mada, A.C. Characterization of Water Extractable Arabinoxylans from a Spring Wheat Flour: Rheological Properties and Microstructure. *Molecules* **2013**, *18*, 8417–8428. [[CrossRef](#)]
35. Schendel, R.R.; Meyer, M.R.; Bunzel, M. Quantitative Profiling of Feruloylated Arabinoxylan Side-Chains from Gramineous Cell Walls. *Front. Plant Sci.* **2016**, *6*, 113. [[CrossRef](#)] [[PubMed](#)]
36. Martínez-López, A.L.; Carvajal-Millan, E.; Lizardi-Mendoza, J.; López-Franco, Y.L.; Rascon-Chu, A.; Salas-Muñoz, E.; Ramírez-Wong, B. Ferulated Arabinoxylans as by-Product from Maize Wet-Milling Process: Characterization and Gelling Capability. In *Maize Cultivation, Uses and Health Benefits*; Nova Science Publishers, Inc.: Hauppauge, NY, USA, 2012; pp. 65–74.
37. Xiang, Z.; Anthony, R.; Tobimatsu, Y.; Runge, T. Emulsifying properties of an arabinoxylan–protein gum from distillers’ grains and the co-production of animal feed. *Cellulose* **2014**, *21*, 3623–3635. [[CrossRef](#)]
38. Irvani, S.; Fitchett, C.S.; Georget, D.M. Physical characterization of arabinoxylan powder and its hydrogel containing a methyl xanthine. *Carbohydr. Polym.* **2011**, *85*, 201–207. [[CrossRef](#)]
39. Kacuráková, M.; Ebringerová, A.; Hirsch, J.; Hromádková, Z. Infrared study of arabinoxylans. *J. Sci. Food Agric.* **1994**, *66*, 423–427. [[CrossRef](#)]
40. Sene, C.; McCann, M.C.; Wilson, R.H.; Grinter, R. Fourier-Transform Raman and Fourier-Transform Infrared Spectroscopy (An Investigation of Five Higher Plant Cell Walls and Their Components). *Plant Physiol.* **1994**, *106*, 1623–1631. [[CrossRef](#)]
41. Robert, P.; Marquis, M.; Barron, C.; Guillon, F.; Saulnier, L. FT-IR Investigation of Cell Wall Polysaccharides from Cereal Grains. Arabinoxylan Infrared Assignment. *J. Agric. Food Chem.* **2005**, *53*, 7014–7018. [[CrossRef](#)]
42. Martínez-López, A.; Carvajal-Millan, E.; Rascón-Chu, A.; Márquez-Escalante, J.; Martínez-Robinson, K. Gels of ferulated arabinoxylans extracted from nixtamalized and non-nixtamalized maize bran: Rheological and structural characteristics. *CyTA J. Food* **2013**, *11*, 22–28. [[CrossRef](#)]
43. Hatfield, R.D.; Ralph, J. Modelling the feasibility of intramolecular dehydrodiferulate formation in grass walls. *J. Sci. Food Agric.* **1999**, *79*, 425–427. [[CrossRef](#)]
44. Mendez-Encinas, M.A.; Carvajal-Millan, E.; Rascón-Chu, A.; Astiazarán-García, H.; Valencia-Rivera, D.E.; Brown, F.; Alday, E.; Velazquez, C. Arabinoxylan-Based Particles: In Vitro Antioxidant Capacity and Cytotoxicity on a Human Colon Cell Line. *Medicina* **2019**, *55*, 349. [[CrossRef](#)]
45. Anderson, C.; Simsek, S. What Are the Characteristics of arabinoxylan gels? *Food Nutr. Sci.* **2018**, *9*, 818–833. [[CrossRef](#)]
46. Ghayempour, S.; Mortazavi, S.M. Fabrication of micro–nanocapsules by a new electrospraying method using coaxial jets and examination of effective parameters on their production. *J. Electrostat.* **2013**, *71*, 717–727. [[CrossRef](#)]
47. Kim, J.; Moon, M.J.; Kim, D.Y.; Heo, S.H.; Jeong, Y.Y. Hyaluronic Acid-Based Nanomaterials for Cancer Therapy. *Polymers* **2018**, *10*, 1133. [[CrossRef](#)]
48. Mohammed, M.A.; Syeda, J.T.M.; Wasan, K.M.; Wasan, E. An Overview of Chitosan Nanoparticles and Its Application in Non-Parenteral Drug Delivery. *Pharmaceutics* **2017**, *9*, 53. [[CrossRef](#)]
49. Sarmiento-de, B.; Ribeiro, A.J.; Veiga, F.; Sampaio, P.; Neufeld, R.; Ferreira, D. Alginate/Chitosan Nanoparticles are Effective for Oral Insulin Delivery. *Pharm. Res.* **2007**, *24*, 2198–2206. [[CrossRef](#)] [[PubMed](#)]

50. Bhatia, M.; Ahuja, M. Psyllium arabinoxylan: Carboxymethylation, characterization and evaluation for nanoparticulate drug delivery. *Int. J. Biol. Macromol.* **2015**, *72*, 495–501. [[CrossRef](#)]
51. Huang, X.; Dai, Y.; Cai, J.; Zhong, N.; Xiao, H.; McClements, D.J.; Hu, K. Resveratrol encapsulation in core-shell biopolymer nanoparticles: Impact on antioxidant and anticancer activities. *Food Hydrocoll.* **2017**, *64*, 157–165. [[CrossRef](#)]



© 2020 by the authors. Licensee MDPI, Basel, Switzerland. This article is an open access article distributed under the terms and conditions of the Creative Commons Attribution (CC BY) license (<http://creativecommons.org/licenses/by/4.0/>).